Journal of Power Sources 205 (2012) 63–70

Contents lists available at SciVerse ScienceDirect

Journal of Power Sources

journal homepage: www.elsevier.com/locate/jpowsour

Carbon supported palladium hollow nanospheres as anode catalysts for direct borohydride-hydrogen peroxide fuel cells

Lanhua Yi, Yunfeng Song, Xianyou Wang*, Liling Yi, Jiafeng Hu, Guo Su, Wei Yi, Hailong Yan

Key Laboratory of Environmentally Friendly Chemistry and Applications of Ministry of Education, School of Chemistry, Xiangtan University, Hunan 411105, PR China

ARTICLE INFO

Article history:
Received 1 October 2011
Received in revised form
10 December 2011
Accepted 1 January 2012
Available online 20 January 2012

Keywords:
Pd hollow nanospheres
Borohydride oxidation
Anode electrocatalyst
Direct borohydride-hydrogen peroxide fuel cell

ABSTRACT

Carbon supported Pd hollow nanospheres (HN-Pd/C) are prepared by employing cobalt nanoparticles as sacrificial templates at room temperature in aqueous solution, and used as the anode electrocatalyst for direct borohydride-hydrogen peroxide fuel cell (DBHFC). The physical and electrochemical properties of the as-prepared nanospherical electrocatalysts are investigated by X-ray diffraction (XRD), transmission electron microscopy (TEM), energy dispersive X-ray spectroscopy (EDS), linear sweep voltammetry (LSV), chronoamperometry (CA), chronopotentiometry (CP) and fuel cell test. The results show that the Pd nanospheres supported on the carbon are coreless and composed of a series of Pd nanoparticles with the average crystallite size of about 3.8 nm. Besides, the HN-Pd/C exhibits distinctly higher electrocatalytic activity for BH_4^- electrooxidation than the carbon supported Pd solid nanoparticles (SN-Pd/C), and the DBHFC using HN-Pd/C as anode electrocatalyst shows as high as 48.4 mW cm^{-2} power densities at a discharge current density of 54.8 mA cm^{-2}. Therefore, the HN-Pd/C catalyst can apparently improve the catalytic activity of BH_4^- electrooxidation and imply a promising application in the DBHFC.

1. Introduction

In recent years, direct borohydride fuel cell (DBFC) has been widely studied and considered as one of the most promising power sources for portable and mobile applications, because it has no catalytic poisoning and is more environmentally friendly [1–4]. Usually, a DBFC employs an alkaline solution of sodium borohydride ($NaBH_4$) as fuel and oxygen or hydrogen peroxide as oxidant. As a nontoxic solid state fuel, sodium borohydride has many advantages over hydrogen, *e.g.* easily transport, convenient storage, high hydrogen content (weight content of 10.6%), high capacity (5.7 Ah g^{-1}), high volumetric energy density (7314 Wh L^{-1}), as well as gravimetric energy density (7100 Wh kg^{-1}).

The anode reaction of the DBFC is the direct oxidation of borohydride in alkaline medium:

$$BH_4^- + 8OH^- \rightarrow BO_2^- + 6H_2O + 8e^- \quad E^0_{anode} = -1.24\,V\ vs.\ SHE \tag{1}$$

The cathode reaction with oxygen as the oxidant is written as:

$$O_2 + 2H_2O + 4e^- \rightarrow 4OH^- \quad E^0_{cathode} = 0.40\ V\ vs.\ SHE \tag{2}$$

The overall fuel cell reaction is:

$$BH_4^- + 2O_2 \rightarrow BO_2^- + 2H_2O \quad E^0_{cell} = 1.64\,V\ vs.\ SHE \tag{3}$$

The theoretical cell voltage is 1.64 V. However, when the hydrogen peroxide in an acid electrolyte instead of oxygen is employed as the oxidant at the cathode, it can yield higher cell potential and energy density:

$$H_2O_2 + 2H^+ + 2e^- \rightarrow 2H_2O \quad E^0_{cathode} = 1.77\,V\ vs.\ SHE \tag{4}$$

In combination with the direct oxidation of borohydride and the reduction of hydrogen peroxide, it gives a theoretical equilibrium cell voltage of 3.01 V and presents a high energy density. Over cell reaction is as follows:

$$BH_4^- + 4H_2O_2 \rightarrow BO_2^- + 6H_2O \quad E^0_{cell} = 3.01\,V \tag{5}$$

Besides, compared with DBFC using oxygen as the oxidant at the cathode, direct borohydride-hydrogen peroxide fuel cell (DBHFC) using hydrogen peroxide in an acid electrolyte as the oxidant has many other advantages in the theoretical and practical aspects [5–7].

However, one of the major challenges to widespread commercialization of DBHFC is the high cost of the anode electrocatalyst. In the past years, different metals have been studied as the alternative anode electrocatalyst for DBFC, such as Pt [8–10], Au [9–11], Pd [12], Ag [13], Ni [14], Zn [15], Os [16] and hydrogen storage alloys [17]. Among these metals, Pt and Au are more attractive than other metals as anode catalysts for DBFC [8–11]. However, due to the

* Corresponding author. Tel.: +86 731 5829060; fax: +86 731 58292061.
E-mail address: wxianyou@yahoo.com (X. Wang).

0378-7753/$ – see front matter © 2012 Elsevier B.V. All rights reserved.
doi:10.1016/j.jpowsour.2012.01.017

limited natural storage resulting in high cost of Pt and Au catalysts, the usage of Pt and Au in DBHFC has to be reduced before this technology can be commercialized.

In recent years, palladium (Pd) has been regarded as one of the most active metal for oxygen reduction reaction (ORR) [18], due largely to its relatively abundant reserve on earth and may display a similar catalytic activity to Pt. Besides, alloying Pd with a second metal cannot only enhances the electrocatalytic activity, but also reduces the cost of the catalyst [19–21]. However, the alloy catalysts usually show poor long-term stability due to the dissolution of non-noble metal, which hampers their final application.

During the past decade, it has been proposed a galvanic replacement method for preparation of bimetallic catalyst materials. The method is based on the spontaneous deposition reaction of noble metal (*e.g.* Pt, Au, Pd, *etc.*) on non-noble metal (*e.g.* Co, Ni, Cu, Pb, *etc.*) surface layers. The obtained catalysts have the noble metal dominated in the outer layers. The driving force for this spontaneous deposition reaction is the positive difference between the equilibrium potential of noble metal in contact with its solvated ions and the non-noble metal [22]. The spontaneous deposition reaction is a surface controlled reaction and the total amount of deposited noble metals is defined by stoichiometry of the redox reaction as well as the structure of the non-noble metals [22]. Adžić and co-workers [22–30] investigated a Cu UPD (the underpotential deposition) monolayer electrodeposited on a noble metal substrate (*e.g.* Pd, Au, Ru or Pt, *etc.*), which is fully replaced by one or more other noble metals (*e.g.* Au, Pt, Pd, Ir, Ru, Rh, Re, Os, *etc.*). The replacement reaction results in noble–noble metal interactions in the outer catalyst layers and significant decrease in the second noble metal loading. Kokkinidis, Tegou and Sotiropoulos [31–38] further developed this idea, they investigated the substrate consisting of electrodeposited non-noble metal multilayers (*e.g.* Pb, Cu, Fe, Co, Ni, *etc.*) and its surface layers are replaced by the noble metal (*e.g.* Pt, Au). The noble–non-noble metal interactions were obtained in the outer layers of the latter catalysts.

More recently, the materials with hollow metal nanostructures have attracted extensive interest due to their distinguished physical and chemical properties which are resulted from their special shape and composition. The materials not only exhibit high catalytic performance and utilization efficiency for their relatively lower densities and higher surface areas than those of their solid counterparts, but also reduce the cost of the catalyst. Although Pd hollow nanosphere catalysts have been used as the electrocatalyst for the oxidation of formic acid in direct formic acid fuel cell (DFAFC) [39], the electrooxidation of BH_4^- on the carbon-supported Pd hollow nanospheres was barely reported to the best of our knowledge. In this paper, the Pd hollow nanospheres were prepared by the spontaneous replacement reaction between Co nanoparticles and $PdCl_4^{2-}$ ions, and then Pd hollow nanospheres were dispersed on Vulcan XC-72R carbon. Finally, the HN-Pd/C was obtained. The electrooxidation behavior of BH_4^- on HN-Pd/C electrode was investigated by electrochemical techniques. Moreover, the performance of the DBHFC employing HN-Pd/C as anode catalyst and carbon supported Pt nanoparticles (Pt/C) as cathode catalyst was studied in detail.

2. Experimental

2.1. Materials

All chemical reagents were analytical grade and used directly as received without further purification. Cobalt chloride ($CoCl_2$), palladium (II) chloride ($PdCl_2$), sodium borohydride ($NaBH_4$), sodium citrate were purchased from Sigma-Aldrich, Vulcan XC-72R carbon ($240\ m^2\ g^{-1}$) was obtained from Cabot Corp., USA. Nafion solution (5 wt.%) and Nafion 117 membrane were provided by DuPont Corp., USA. Double distilled water of 18 MΩ cm was used to prepare the solutions.

2.2. Preparation of HN-Pd/C electrocatalyst

The Co nanoparticles were fabricated by adding an aqueous solution of $CoCl_2$ (0.4 M; 0.3 ml) to the mixed solution (300 ml) of $NaBH_4$ (4 mM) and sodium citrate (0.67 mM) with violently stirring. With immediate hydrogen evolution, the solution turned from colorless to brown, indicating the formation of Co nanoparticles. In order to completely decompose the residual sodium borohydride, above solution was allowed to stir continuedly under argon for an additional 1 h. Besides, to avoid the oxidation of the prepared Co nanoparticles by atmospheric oxygen, high-purity argon was bubbled through the solution during the whole procedure. While maintaining argon flow, the resulting solution was immediately added to an aqueous H_2PdCl_4 solution (5 mM; 15 ml) under magnetic stirring. Then, the solution changed from brown to black, suggesting that a trans-metallation reaction occurred according to Eq. (6):

$$Co + PdCl_4^{2-} = Pd + CO^{2+} + 4Cl^- \quad (6)$$

After 1 h, to ensure that Co nanoparticles were oxidized by $PdCl_4^{2-}$, the argon flow was stopped and the vessel was opened at ambient conditions under stirring to oxidize the remaining cobalt metal left in solution. After another more 1 h, Vulcan XC-72R carbon (31.93 mg) was then added to the above solution. After continuedly stirred for 3 h, the resulting catalyst was filtered and washed with deionized water until no Cl^- was detected, finally dried for 12 h at 80 °C in vacuum to obtain HN-Pd/C catalysts. The amount of Pd is 20 wt.% of total catalyst weight.

2.3. Preparation of SN-Pd/C electrocatalyst

In this study, SN-Pd/C and Pt/C catalysts were prepared according to a modified $NaBH_4$ reduction method previously reported [40]. In brief, the required amounts of H_2PdCl_4 or H_2PtCl_6, carbon and polyvinylpyrrolidone (PVP) were added to 100 ml deionized (DI) water under vigorous stirring, and then it was kept to stir for 30 min. The pH of the mixed solution was adjusted to 10 by adding 3 M NaOH solution, and 1 ml of 1 M $NaBH_4$ was added dropwise. After an additional 24 h stirring, the resulting catalyst was filtered and washed with deionized water until no Cl^- was detected, finally dried for 12 h at 80 °C in vacuum to obtain SN-Pd/C or Pt/C catalysts. For each catalyst, the amount of metal is 20 wt.% of total catalyst weight.

2.4. Material characterization

A diffractometer (D/MAX-3C) was employed using Cu Kα radiation (λ = 0.154056 nm) and a graphite monochromator at 50 kV, 100 mA to obtain XRD spectra of the samples. The 2θ angular regions between 10° and 90° were explored at a scan rate of $5^\circ\ min^{-1}$.

The structure and morphology of SN-Pd/C and HN-Pd/C catalysts were examined by TEM, using a Jeol 3010 microscope operated at 300 kV. For TEM analysis, samples were prepared by placing one or two drops of nanoparticles solution onto the carbon-coated copper grid and drying it in air at room temperature.

Elemental analysis of the as-prepared catalysts was performed by EDS system, which was attached to the JEOL JSM-6360 scanning electron microscopy.

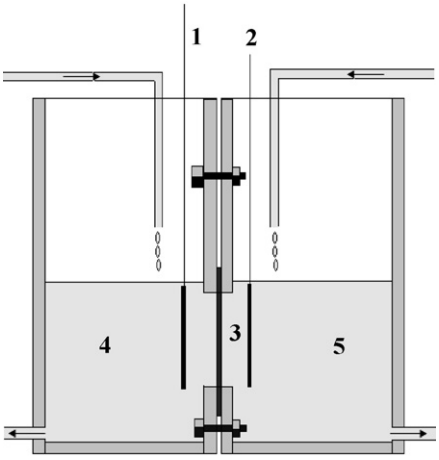

Fig. 1. Schematic illustration of DBHFC. (1) Anode catalyst, (2) cathode catalyst, (3) the activated Nafion 117 membrane, (4) 1 M $NaBH_4$ + 3.0 M NaOH, (5) 2 M H_2O_2 + 0.5 M H_2SO_4.

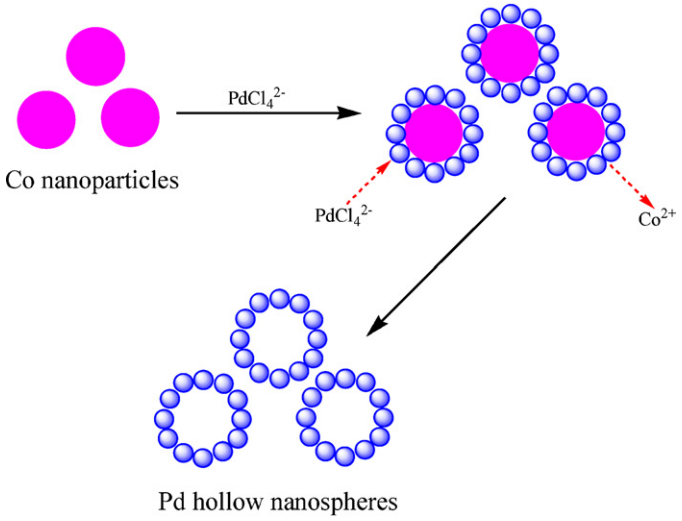

Fig. 2. Schematic illustration of the designed and prepared procedure of the Pd hollow nanospheres.

2.5. Electrochemical characterization

Electrochemical measurements were performed using CHI660A Electrochemistry Workstation and a typical three-electrode one-compartment electrolysis cell. The HN-Pd/C or SN-Pd/C was used as working electrode, a Ni foam mesh with 3 cm × 5 cm as counter electrode and an Ag/AgCl, KCl_{std} as the reference electrode. The electrolyte was 0.1 M $NaBH_4$ + 3.0 M NaOH. The working electrode was prepared as follows: 10 mg of HN-Pd/C or SN-Pd/C powder was dispersed by ultrasonic for 2 h in 1 ml blending solution of 0.25 ml 5 wt.% Nafion solution and 0.75 ml de-ionized water. Then 5 μl of slurry was pasted on the surface of the glassy carbon (GC) electrode (3 mm in diameter) which was polished to mirror by 0.5 μm alumina and sonicated 15 min prior to use. The dispersed catalyst on the GC surface was dried for 5 h at ambient temperature. The loading mass of catalyst on electrode was 0.7 mg cm^{-2} and actual metal loading mass on electrode is 0.14 mg cm^{-2}.

2.6. Fuel cell test

The catalysts ink was made by mixing isopropyl alcohol with 7 wt.% of nafion solution and carbon supported catalysts. Then the ink were coated onto a stainless steel gauze resulting in a 4.5 mg cm^{-2} loading, and actual metal loading mass on electrode is 0.9 mg cm^{-2}. The catalyst electrodes were pressed at 10 MPa for 1 min after drying at 50 °C in vacuum for 8 h.

The cell performance was tested against a HN-Pd/C or a SN-Pd/C anode electrode and the cathode is a Pt/C electrode. A schematic diagram of the experimental set-up was shown in Fig. 1. A Nafion 117 membrane was used to separate the anolyte and catholyte. The anolyte is composed of 1 M $NaBH_4$ + 3 M NaOH, and the catholyte is composed of 2 M H_2O_2 + 0.5 M H_2SO_4. The fresh anolyte and catholyte were continuously supplied and withdrawn from the cell at 0.7 ml min^{-1}, respectively. The load was applied in steps of 5 mA within the range of 0–120 mA. Each step lasted 2 min and the current was continuously applied from one value to next without disconnecting the cell. The electrochemical testing of the cell was performed using a battery testing system (BTS-51800, Neware Technology Co. Ltd., China). Power densities were calculated from the applied current and steady state potential.

3. Results and discussion

3.1. Physical characterizations

The Pd hollow nanospheres can be prepared on the basis of the replacement reaction between Co nanoparticles and H_2PdCl_4, which is described in detail in Eq. (6). During preparation process, synthesis of Co nanoparticle is a key step. Generally speaking, when the color of the solution changes from transparent to dark, it indicates the formation of Co nanoparticles. Citrate is present as a capping agent to prevent the growth of Co nanoparticles through repulsive forces between negatively charged Co nanoparticles. Ar is bubbled through the solution during the procedure to avoid the oxidation of Co nanoparticles in the presence of atmospheric oxygen. For trans-metallation reaction in Eq. (6), the standard reduction potential of $PdCl_4^{2-}$/Pd (0.591 V *vs.* the standard hydrogen electrode (SHE)) is much higher than that of Co^{2+}/Co (−0.227 V *vs.* SHE). As a result, when the solution containing Co nanoparticles is added to H_2PdCl_4 solution, $PdCl_4^{2-}$ ions absorbed rapidly on the surface of the Co nanoparticles, and then the Co nanoparticles are immediately oxidized into Co^{2+} due to the large potential difference between two redox couples. This replacement reaction occurs rapidly. The Pd grows into small nanoparticles and evolves into a thin shell around the Co nanoparticles. As the reaction continued, Co^{2+} and $PdCl_4^{2-}$ continuously diffused through the shell until the Co cores were completely consumed and a hollow Pd nanoshell was formed. The shell should have an incomplete porous structure because Co^{2+} and $PdCl_4^{2-}$ continuously diffuse across it [41,42]. The schematic mechanism in this process is shown in Fig. 2.

In order to investigate the structure of the hollow Pd nanoshell, the X-ray diffraction (XRD) patterns of SN-Pd/C and HN-Pd/C catalysts were shown in Fig. 3. The wide diffraction peak located at a 2θ value of about 25.0° is attributed to carbon (0 0 2) crystal face, which matches well with the standard C diffraction peak (JCPDS No. 75-1621). And the other four strong diffraction peaks positioned at 40.1°, 46.3°, 68.1° and 81.9° correspond to the (1 1 1), (2 0 0), (2 2 0), and (3 1 1) facets of Pd crystal, respectively, which are in good agreement with the standard card of cubic Pd (JCPDS No. 88-2335). The diffraction peak for Pd (1 1 1) is used to estimate the Pd particle size by the Scherrer formula [43]:

$$D = \frac{0.9\lambda}{B\ \cos\theta} \quad (7)$$

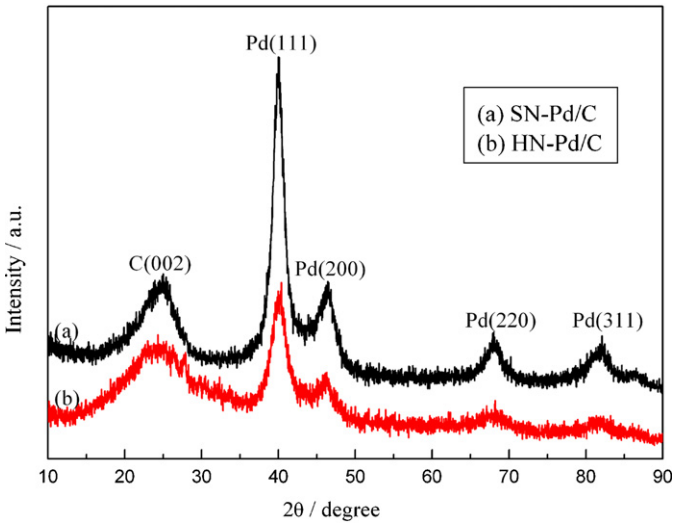

Fig. 3. XRD patterns of SN-Pd/C and HN-Pd/C.

where D is average particle size, nm, λ is the X-ray wavelength (1.54056 Å for Cu Kα radiation), B is the full width at half-maximum in radians (FWHM) and θ is the angle of Pd (1 1 1) peak. The calculated average size of the Pd nanoparticles which form the shell of Pd hollow nanospheres is about 3.8 nm, while the average size of Pd solid nanoparticles dispersed on carbon is about 5.0 nm. No cobalt nanocrystals peaks were found, indicating complete re-dissolving of cobalt into solution after stopping Ar bubbling.

Fig. 4 is typical TEM images of SN-Pd/C (Fig. 4a) and HN-Pd/C (Fig. 4b and c). As shown in Fig. 4a, most of the solid Pd nanoparticles are spherical in shape without aggregation and have a narrow particle size distribution. The metal nanoparticles are uniformly dispersed on the surface of carbon with the mean diameter of approximate 5 nm, and the result is well consistent with the XRD result (5.0 nm). Fig. 4b and c are the TEM and HR-TEM images of HN-Pd/C catalyst. It was found that the Pd nanoparticles with uniform size were homogeneously distributed on the surface of Vulcan XC-72R carbon, and they assembled together and formed the hollow spherical shells. Besides, it can be seen from Fig. 4c that the centers of the Pd nanospheres were much brighter than the edges, indicating that the nanosphere was actually a hollow spherical structure. The average size of the Pd hollow nanosphere estimated from the TEM image is about 20 nm, and the average thickness of the shell is about 4 nm. Apparently, each Pd hollow nanosphere is assembly of many Pd nanoparticles with about 4 nm diameter, and the result also is well consistent with the XRD result (3.8 nm). In addition, the shell of the Pd hollow nanospheres was incomplete and porous, this feature will reciprocate the Pd hollow nanospheres a high specific surface area [41].

The chemical composition of SN-Pd/C and HN-Pd/C catalysts was determined by EDS (Fig. 5). It can be seen from Fig. 5 that two main peaks assigned to carbon and Pd can be observed in both EDS

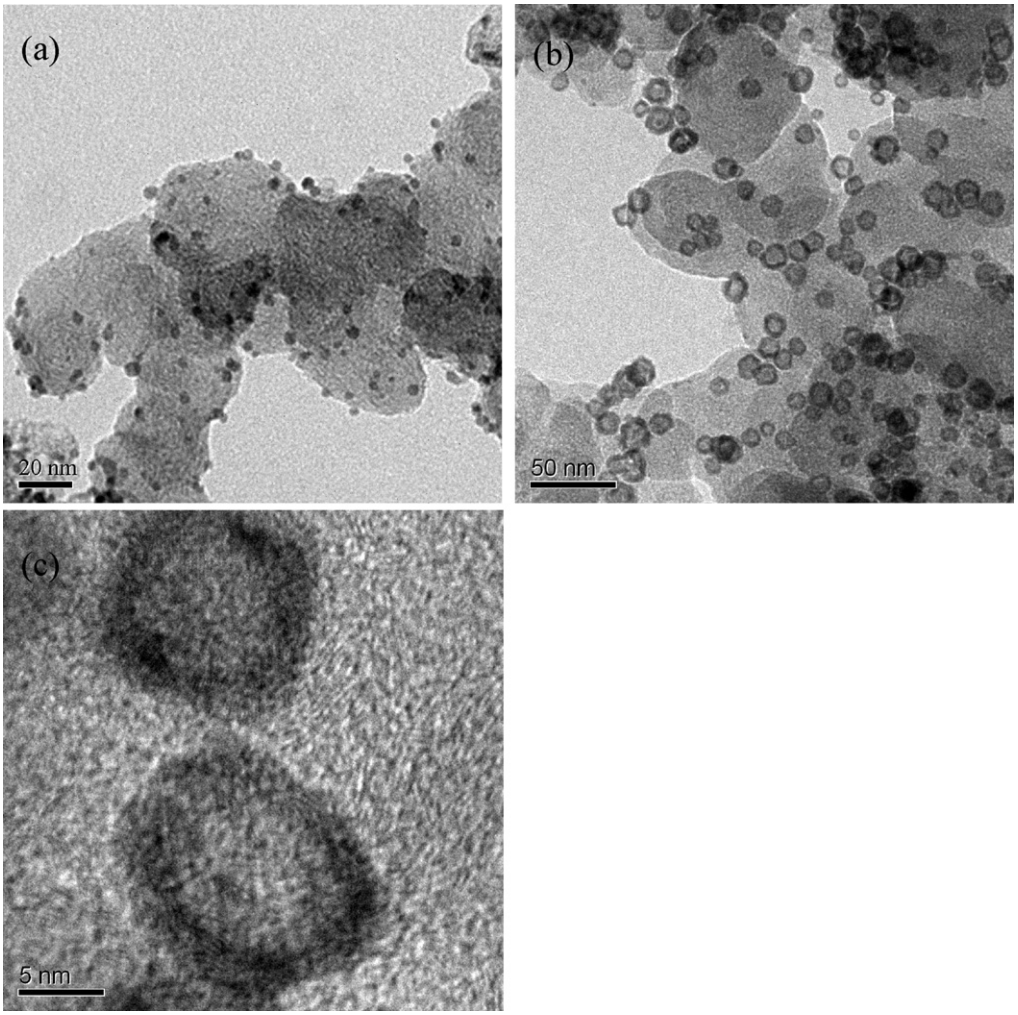

Fig. 4. TEM images of SN-Pd/C (a) and HN-Pd/C (b, c).

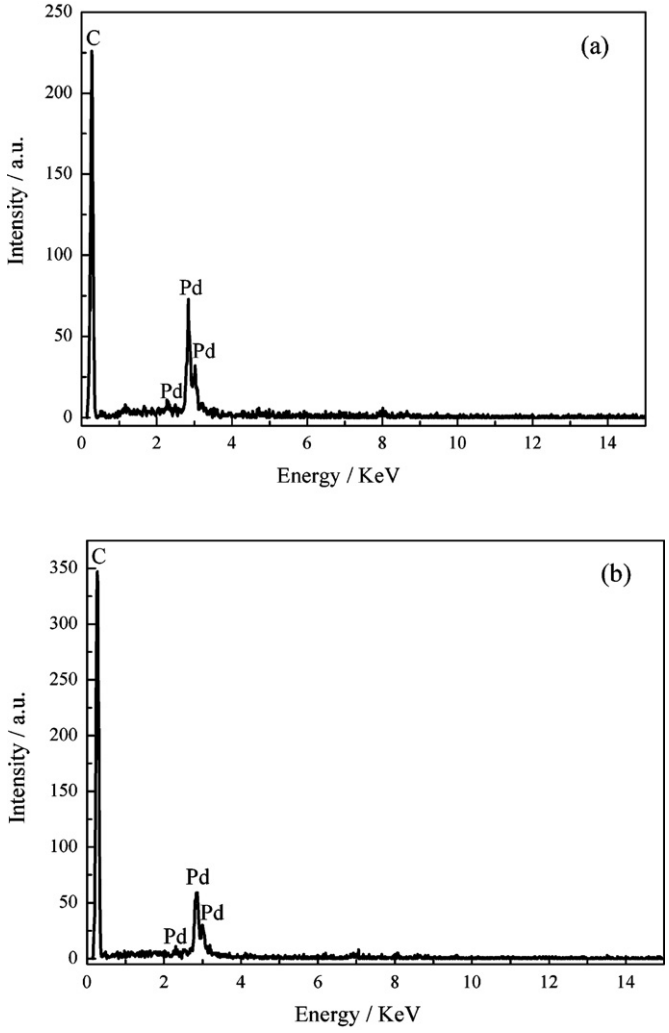

Fig. 5. EDS spectra of SN-Pd/C (a) and HN-Pd/C (b).

spectra corresponding to SN-Pd/C (Fig. 5a) and HN-Pd/C (Fig. 5b) catalysts (a much higher peak is assigned to carbon, and a lower peak near 3 keV is assigned to Pd), indicating that both SN-Pd/C and HN-Pd/C catalysts are composed of Pd and carbon. The Pd mass percentage of SN-Pd/C and HN-Pd/C catalysts is 20.2% and 19.0%, respectively, which is coincided with the ratio of Pd to carbon in the starting mixture. As to HN-Pd/C catalyst, there is no signal from Co in the EDS spectra, which indicates that the Co nanoparticles have been depleted thoroughly during the process. This phenomenon is also consistent with the XRD results.

3.2. Electrochemically active surface area estimation

The most common and convenient approach to the determination of the electrochemically active surface area (ECSA) of Pd electrodes involves the measurements of the charge of formation and reduction of PdO [44,45]. Fig. 6 shows cyclic voltammetric curves of the SN-Pd/C and HN-Pd/C catalyst electrodes in 0.5 M H_2SO_4 solution from −0.2 V to 1.4 V *vs.* Ag/AgCl, KCl_{std}. at a scan rate of 50 mV s^{-1}. As shown in Fig. 6, the PdO reduction peak of HN-Pd/C is larger than that of SN-Pd/C. The charge density of 0.424 mC cm^{-2} is associated to the reduction of the formed PdO monolayer [44,45], and the calculated ECSA value of Pd hollow nanospheres dispersed on carbon, obtained by integration of the PdO reduction zone on the voltammogram presented in Fig. 6, is closed to 31.6 m^2 g^{-1}, which is higher than that of Pd solid nanoparticles dispersed on

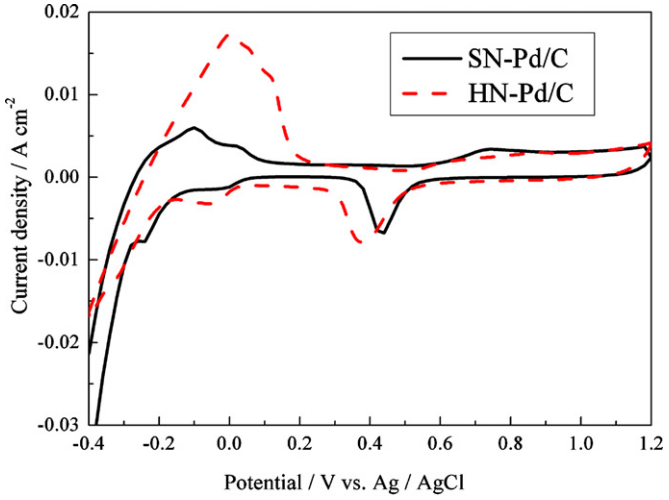

Fig. 6. Cyclic voltammograms of SN-Pd/C and HN-Pd/C electrodes in Ar-saturated 0.5 M H_2SO_4 solution at a scan rate of 50 mV s^{-1}.

carbon (22.6 m^2 g^{-1}), indicating that the enhanced electrochemical activity of Pd hollow nanospheres can be obtained.

3.3. Linear sweep voltammetry study

Fig. 7 show the linear sweep voltammograms (LSV) recorded using SN-Pd/C and HN-Pd/C electrodes in 0.1 M $NaBH_4$ + 3.0 M NaOH solution at a scan rate of 20 mV s^{-1} in the potential range of −1.2 V to 0.6 V *vs.* Ag/AgCl, KCl_{std}. The current densities of LSV plots in Fig. 7a and b were calculated on the basis of the geometric area and electrochemically active surface area, respectively. As shown in Fig. 7a, the BH_4^- oxidation peak on HN-Pd/C electrode appears at −0.653 V, which is much more negative than that on SN-Pd/C electrode (−0.318 V), and the peak current density on HN-Pd/C electrode is 40.49 mA cm^{-2}, much higher than that on the SN-Pd/C electrode (34.28 mA cm^{-2}). The high oxidation peak current density for the HN-Pd/C electrode may be directly related to the catalytic activity of Pd hollow nanospheres. Therefore, it can be expected that the catalytic activity of HN-Pd/C electrode will be higher than SN-Pd/C electrode.

Furthermore, an accurate estimation of intrinsic electrocatalytic activity of the catalysts could be made if current densities are calculated based on the electrochemically active surface area (as estimated in Section 3.2) [37]. The current densities of LSV plots in Fig. 7b were calculated on the basis of the electrochemically active surface area. As shown in Fig. 7b, even after correction for the increased electrochemically active surface area of the HN-Pd/C electrode, the current density corresponding to HN-Pd/C electrode is 0.93 mA cm^{-2}, which is still close to that of SN-Pd/C electrode (1.05 mA cm^{-2}). This result indicates that the HN-Pd/C and SN-Pd/C catalysts have similar intrinsic catalytic activity. As a result, the much higher electrocatalytic activity and current density observed on HN-Pd/C electrode (Fig. 7a) could be attributed to the increase in the electrochemically active surface area.

3.4. Chronopotentiometry

By analogy with the constant current operation of a direct borohydride fuel cell, chronopotentiometry could provide further relevant information. Fig. 8 depicts the chronopotentiometry of BH_4^- oxidation on the SN-Pd/C and HN-Pd/C electrodes at a current density of 8.5 mA cm^{-2} in the solution of 0.1 M $NaBH_4$ + 3.0 M NaOH. Apparently, the overpotential on the HN-Pd/C electrode is clearly lower than that on the SN-Pd/C electrode. Therefore, after 120 s, the

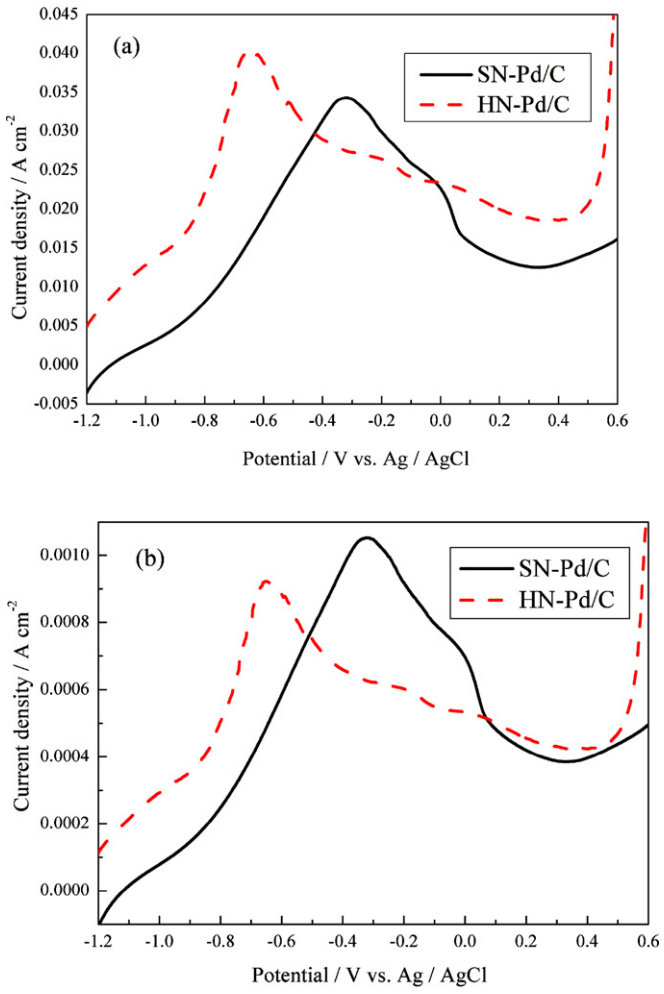

Fig. 7. Linear sweep voltammograms of SN-Pd/C and HN-Pd/C electrodes in 0.1 M $NaBH_4$ + 3.0 M NaOH solution at a scan rate of 20 mV^{-1}. (a) Current density is given based on the geometric area, (b) current density is given based on the electrochemically active surface area.

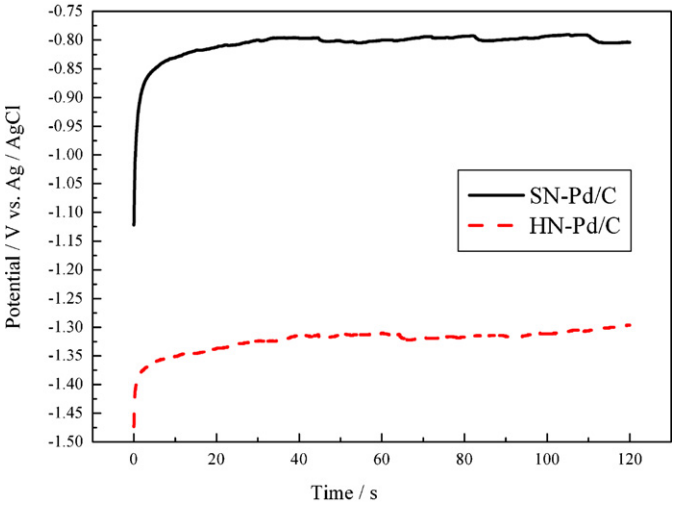

Fig. 8. Chronopotentiometry curves of SN-Pd/C and HN-Pd/C electrodes in 0.1 M $NaBH_4$ + 3.0 M NaOH solution. Current step from 0 to 8.5 mA cm^{-2}.

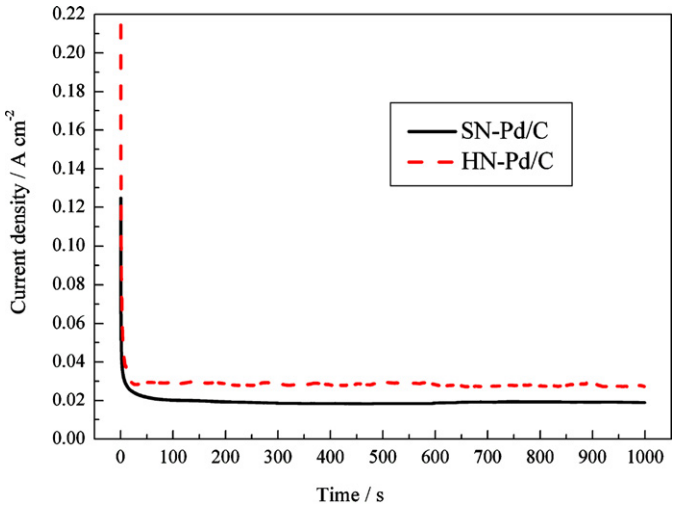

Fig. 9. Chronoamperometry curves of SN-Pd/C and HN-Pd/C electrodes in 0.1 M $NaBH_4$ + 3.0 M NaOH solution. Potential step from −1.2 to −0.2 V *vs.* Ag/AgCl.

operating potential of HN-Pd/C electrode was −1.296 V, which is much more negative than that of the SN-Pd/C electrode (−0.804 V). Generally speaking, a lower overpotential is an indication of better electroactivity, and the more negative electrode potential will be beneficial to occurrence of oxidation reaction. This is also attributed to the microstructure of Pd hollow nanospheres. The incomplete and porous hollow structure will provide much more active center for electrocatalytic reaction due to large specific surface area and is more favorable for mass transfer of liquid fuel toward active site, and thus the kinetics of BH_4^- electrooxidation can be improved [8]. It is reported recently that BH_4^- oxidation on Pd/C and Pd/MWCNT catalysts displayed near 4e reaction mechanisms [12]. Since the carbon support does not participate in the electrocatalytic oxidation reaction, we consider that the catalytic active materials in Pd/C and Pd/MWCNT are Pd nanoparticles. Therefore, we tentatively assigned a 4e reaction mechanism to the BH_4^- oxidation on HN-Pd/C catalyst.

3.5. Chronoamperometry

Chronoamperometric technique is an effective method to evaluate the electrocatalytic activity and stability of catalyst material. Fig. 9 shows the chronoamperometric responses on SN-Pd/C and HN-Pd/C electrodes in 0.1 M $NaBH_4$ + 3.0 M NaOH solution from −1.2 to −0.2 V. It can be found that both electrocatalysts show current decay during the process of BH_4^- electrooxidation. The current decay rate over time on SN-Pd/C electrode is faster than that on HN-Pd/C electrode. After 1000 s, the HN-Pd/C electrode delivers higher final current density (27.30 mA cm^{-2}) than that of the SN-Pd/C electrode (18.89 mA cm^{-2}). During entire experimental, the current density is higher in the case of the HN-Pd/C electrode. This could be an indication that the HN-Pd/C electrode has a higher electrocatalytic activity than the SN-Pd/C electrode, and this result is consistent with that of LSV and CP measurements.

3.6. Fuel cell performance measurement

Fig. 10 shows the changes of the cell voltage and power density as a function of current density at 20 °C using the HN-Pd/C anode catalyst in comparison with SN-Pd/C anode catalyst. The cathode catalysts of both DBHFC systems were Pt/C. The anolyte was 1 M $NaBH_4$ + 3 M NaOH solution, and the catholyte was 2 M H_2O_2 + 0.5 M H_2SO_4 solution according to our previous studies [40,46]. The open circuit voltage (OCV) of the cell is about 1.85 V, which is lower than

Table 1
Characteristic parameters of DBHFCs using SN-Pd/C and HN-Pd/C as anode catalysts at 20 °C.

Example	Open circuit voltage OCV (V)	Current density j (mA cm^{-2})	Peak power density P (mW cm^{-2})
DBHFC with SN-Pd/C as anode	1.866	44.8	36.0
DBHFC with HN-Pd/C as anode	1.839	54.8	48.4

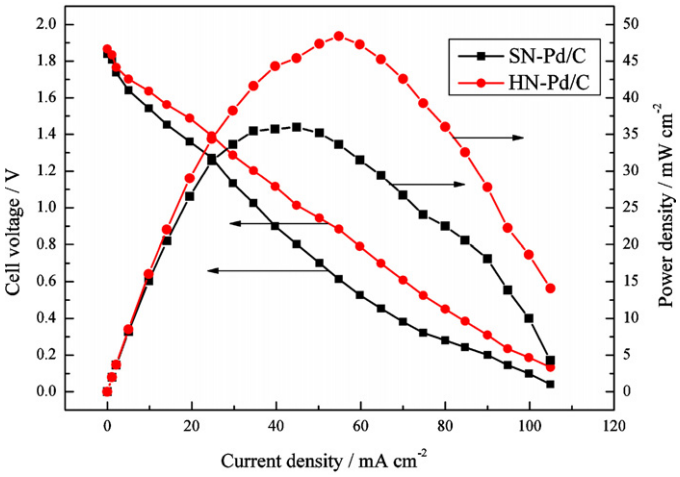

Fig. 10. Cell voltage and power density *vs.* current density for DBHFCs with SN-Pd/C and HN-Pd/C anodes at 20 °C. Anolyte: 1 M $NaBH_4$ + 3 M NaOH, catholyte: 2 M H_2O_2 + 0.5 M H_2SO_4.

the standard cell potential for the DBHFC. The low value is probably caused by mixed potential at the anode and cathode from simultaneous oxidation of BH_4^- ions and hydrogen at the anode and reduction of H_2O_2 and O_2 at the cathode [47]. The behavior of the cell voltage *vs.* current density obtained using HN-Pd/C as anode catalyst shows a similar linear behavior experienced with SN-Pd/C anode catalyst. However, the cell voltage dropped more slowly as the current density increased. For comparison, the characteristic parameters of DBHFCs were tabulated in Table 1. It can be seen from Table 1 that the maximum power density is 48.4 mW cm^{-2} at a discharge current density of 54.8 mA cm^{-2} at 20 °C. Thus, the DBHFC using HN-Pd/C as anode catalyst exhibits superior performance to the one using SN-Pd/C as anode catalyst, and the HN-Pd/C improves potentially the activity of Pd electrocatalysts for the DBHFC.

4. Conclusions

(1) A facile procedure for preparing carbon supported Pd hollow nanospheres catalyst with Co nanoparticles as sacrificial templates was developed. A series of Pd nanoparticles with average diameter of 3.8 nm congregated together and finally formed the Pd hollow nanosphere. Thus, the resultant nanosphere was actually a hollow spherical structure with average diameter of 20 nm, and the shell of the Pd hollow nanospheres was incomplete and porous.
(2) The HN-Pd/C catalyst exhibits much higher electrochemical catalytic activity than SN-Pd/C for BH_4^- oxidation in the alkaline solution. The maximum power density of the DBHFC employing HN-Pd/C as anode catalyst and Pt/C as cathode catalyst was 48.4 mW cm^{-2} at 20 °C.

Therefore, the HN-Pd/C catalyst with high performance and low cost will be a promising anode catalyst for the application of DBHFCs.

Acknowledgments

This work was financially supported by the National Natural Science Foundation of China (Grant nos. 20871101 and 51072173), Doctoral Fund of Ministry of Education of China (Grant no. 20094301110005), the Science and Technology Plan Project of Hunan Province (Grant no. 2010GK3181) and the Scientific Research Fund of Hunan Provincial Education Department (Grant nos. 11A118 and 11C1207).

References

[1] B.H. Liu, Z.P. Li, J. Power Sources 187 (2009) 291–297.
[2] C. Kim, K.J. Kim, M.Y. Ha, J. Power Sources 180 (2008) 114–121.
[3] B.H. Liu, Z.P. Li, S. Suda, J. Power Sources 175 (2008) 226–231.
[4] R. Jamard, J. Salomon, A. Martinent-Beaumont, C. Coutanceau, J. Power Sources 1935 (2009) 779–787.
[5] G.H. Miley, N. Luo, J. Mather, R. Burton, G. Hawkins, L.F. Gu, E. Byrd, R. Gimlin, P.J. Shrestha, G. Benavides, J. Laystrom, D. Carroll, J. Power Sources 165 (2007) 509–516.
[6] N. Luo, G.H. Miley, K.J. Kim, R. Burton, X. Huang, J. Power Sources 185 (2008) 685–690.
[7] C. Ponce de león, F.C. Walsh, A. Rose, J.B. Lakeman, D.J. Browning, R.W. Reeve, J. Power Sources 164 (2007) 441–448.
[8] J.H. Kim, H.S. Kim, Y.M. Kang, M.S. Song, S. Rajendran, S.C. Han, D.H. Jung, J.Y. Lee, J. Electrochem. Soc. 151 (2004) A1039–A1043.
[9] E. Gyenge, Electrochim. Acta 49 (2004) 965–978.
[10] D.A. Finkelstein, N.D. Mota, J.L. Cohen, H.D. Abruña, J. Phys. Chem. C 113 (2009) 19700–19712.
[11] M.V. Mirkin, H. Yang, A.J. Bard, J. Electrochem. Soc. 139 (1992) 2212–2217.
[12] J.Q. Yang, B.H. Liu, S. Wu, J. Power Sources 194 (2009) 824–829.
[13] E. Sanli, B.Z. Uysal, M.L. Aksu, Int. J. Hydrogen Energy 33 (2008) 2097–2104.
[14] J. Ma, Y. Sahai, R.G. Buchheit, J. Power Sources 195 (2010) 4709–4713.
[15] D.M.F. Santos, C.A.C. Sequeira, J. Electrochem. Soc. 157 (2010) B13–B19.
[16] V.W.S. Lam, E.L. Gyenge, J. Electrochem. Soc. 155 (2008) B1155–B1160.
[17] B.H. Liu, M. Chatenet, J. Alloys Compd. 454 (2008) 280–285.
[18] L.M. Vracar, D.B. Sepa, A. Damjanovic, J. Electrochem. Soc. 133 (1986) 1835–1839.
[19] S.J. Guo, S.J. Dong, E.k. Wang, ACS Nano 4 (2010) 547–555.
[20] C.H. Cui, J.W. Yu, H.H. Li, M.R. Gao, H.W. Liang, S.H. Yu, ACS Nano 5 (2011) 4211–4218.
[21] D. Ferrer, A. Torres-Castro, X. Gao, S. Sepúlveda-Guzmán, U. Ortiz-Méndez, M. José-Yacamán, Nano Lett. 7 (2007) 1701–1705.
[22] S.R. Brankovic, J.X. Wang, R.R. Adžić, Surf. Sci. 474 (2001) L173–L179.
[23] S.R. Brankovic, J.X. Wang, Y. Zhu, R. Sabatini, J. McBreen, R.R. Adžić, J. Electroanal. Chem. 524/525 (2002) 231–241.
[24] K. Sasaki, Y. Mo, J.X. Wang, M. Balasubramanian, F. Uribe, J. McBreen, R.R. Adžić, Electrochim. Acta 48 (2003) 3841–3849.
[25] J. Zhang, Y. Mo, M.B. Vukmirovic, R. Klie, K. Sasaki, R.R. Adžić, J. Phys. Chem. B 108 (2004) 10955–10964.
[26] J. Zhang, F.H.B. Lima, M.H. Shao, K. Sasaki, J.X. Wang, R.R. Adžić, J. Phys. Chem. B 109 (2005) 22701–22704.
[27] J. Zhang, M.B. Vukmirovic, K. Sasaki, A.U. Nilekar, M. Mavrikakis, R.R. Adžić, J. Am. Chem. Soc. 127 (2005) 12480–12481.
[28] M.H. Shao, T. Huang, P. Liu, J. Zhang, K. Sasaki, M.B. Vukmirovic, R.R. Adžić, Langmuir 22 (2006) 10409–10415.
[29] M.B. Vukmirovic, J. Zhang, K. Sasaki, A.U. Nilekar, F. Uribe, M. Mavrikakis, R.R. Adžić, Electrochim. Acta 52 (2007) 2257–2263.
[30] F.H.B. Lima, J. Zhang, M.H. Shao, K. Sasaki, M.B. Vukmirovic, E.A. Ticianelli, R.R. Adžić, J. Phys. Chem. C 111 (2007) 404–410.
[31] M. Van Brussel, G. Kokkinidis, I. Vandendael, C. Buess-Herman, Electrochem. Commun. 4 (2002) 808–813.
[32] M. Van Brussel, G. Kokkinidis, A. Hubin, C. Buess-Herman, Electrochim. Acta 48 (2003) 3909–3919.
[33] S. Papadimitriou, A. Tegou, E. Pavlidou, G. Kokkinidis, S. Sotiropoulos, Electrochim. Acta 52 (2007) 6254–6260.
[34] A. Tegou, S. Papadimitriou, E. Pavlidou, G. Kokkinidis, S. Sotiropoulos, J. Electroanal. Chem. 608 (2007) 67–77.
[35] S. Papadimitriou, A. Tegou, E. Pavlidou, S. Armyanov, E. Valova, G. Kokkinidis, S. Sotiropoulos, Electrochim. Acta 53 (2008) 6559–6567.
[36] A. Tegou, S. Armyanov, E. Valova, G. Kokkinidis, S. Sotiropoulos, J. Electroanal. Chem. 623 (2008) 187–196.
[37] A. Tegou, S. Armyanov, E. Valova, O. Steenhaut, A. Hubin, G. Kokkinidis, S. Sotiropoulos, J. Electroanal. Chem. 634 (2009) 104–110.

[38] A. Tegou, S. Papadimitriou, G. Kokkinidis, S. Sotiropoulos, J. Solid State Electrochem. 14 (2010) 175–184.
[39] J.J. Ge, W. Xing, X.Z. Xue, C.P. Liu, T.H. Lu, J.H. Liao, J. Phys. Chem. C 111 (2007) 17305–17310.
[40] L.H. Yi, B.A. Hu, Y.F. Song, X.Y. Wang, G.S. Zou, W. Yi, J. Power Sources 196 (2011) 9924–9930.
[41] H.P. Liang, H.M. Zhang, J.S. Hu, Y.G. Guo, L.J. Wan, C.L. Bai, Angew. Chem. Int. Ed. 43 (2004) 1540–1543.
[42] H.P. Liang, N.S. Lawrence, L.J. Wan, L. Jiang, W.G. Song, T.G.J. Jones, J. Phys. Chem. C 112 (2008) 338–344.
[43] S.X. Zhang, M. Qing, H. Zhang, Y.N. Tian, Electrochem. Commun. 11 (2009) 2249–2252.
[44] M. Grdeń, M. Łukaszewski, G. Jerkiewicz, A. Czerwiński, Electrochim. Acta 53 (2008) 7583–7598.
[45] A.J. Zhang, M. Gaur, V.I. Birss, J. Electroanal. Chem. 389 (1995) 149–159.
[46] P.Y. He, Y. Wang, X.Y. Wang, F. Pei, H. Wang, L. Liu, L.H. Yi, J. Power Sources 196 (2011) 1042–1047.
[47] C. Ponce de león, F.C. Walsh, C.J. Patrissi, M.G. Medeiros, P.R. Bessette, R.W. Reeve, J.B. Lakeman, A. Rose, D. Browning, Electrochem. Commun. 10 (2008) 1610–1613.